Nanoscale

Accepted Manuscript

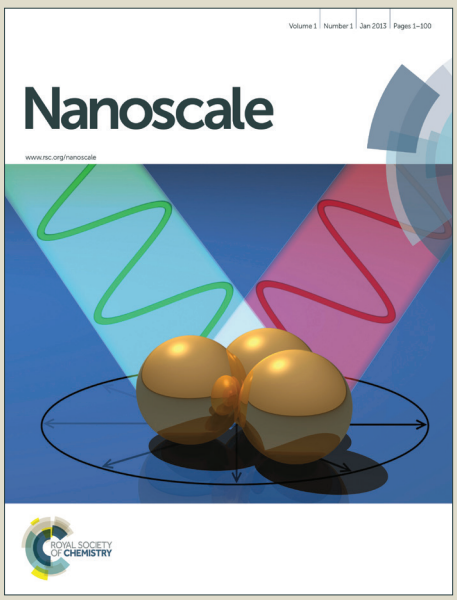

ROYAL SOCIETY OF CHEMISTRY

www.rsc.org/nanoscale

Cite this: DOI: 10.1039/c0xx00000x

www.rsc.org/xxxxxx

FULL PAPER

Three-dimensional hierarchical Te–Si nanostructures

Jae-Hong Lim,[+a] Gyeong-Jin Shin,[+b] Tae-Yeon Hwang,[c] Hyo-Ryoung Lim,[c] Young-In Lee,[d] Kyu-Hwan Lee,[a] Sung-Dae Kim,[e] Min-Wook Oh,[f] Su-Dong Park,[f] Nosang V. Myung*[g] and Yong-Ho Choa*[bcd]

Received (in XXX, XXX) Xth XXXXXXXXX 20XX, Accepted Xth XXXXXXXXX 20XX

DOI: 10.1039/b000000x

Three-dimensional hybrid nanostructures (*i.e.,* Te "nanobranches" on a Si "nanotrunk" or Te "nanoleaves" on a Si "nanotrunk") were synthesized by combining the gold-assisted chemical etching of Si to form Si "nanotrunks" and the galvanic displacement of Si to form Te "nanobranches" or "nanoleaves." By adjusting the composition of the electrolyte used for the galvanic displacement reaction, the shape of the Te nanostructures could be changed from nanoleaves to nanobranches. The Si nanotrunks with Te nanobranches showed stronger luminescent emission in the visible region, with their Raman spectrum having a higher wave number, owing to their grain size being larger. This suggested that the optical and photoelectrochemical properties of Te–Si hybrid nanostructures depend on their shape and size. Using this approach, it should be possible to fabricate various hierarchical nanostructures for use in photoelectronic and photoelectrochemical devices.

Keywords: metal-assisted chemical etching, silicon, nanosphere lithography, galvanic displacement reaction, hybrid nanostructures

1 Introduction

Nanostructures, including nanoparticles, nanowires, nanotubes, and nanofibers, and hybrids of such structures are attractive building blocks for fabricating next-generation electronic, photonic, energy storage and generation, and magnetic devices.[1] The functionality of three-dimensional (3D) complex nanostructures can be enhanced further by engineering the interface and providing a high surface area-to-volume ratio. In particular, 3D "tree-like" or hyperbranched nanostructures are attracting significant interest because of their enhanced structural complexity and functionalities, such as a high surface area, low reflectance, and heterostructured nature.[2,3] Hyperbranched nanostructures of a wide range of materials, including ZnO, GaN, Si, and SnO_2, have been synthesized by vapor-phase or solution-phase growth processes. In these processes, the branches are typically formed by placing secondary seeds (*e.g.*, metal catalysts) on the primary trunk, which results in the growth of branches.[4] Although it has been shown that these processes can be used to form hyperbranched nanostructures, one has to overcome numerous obstacles when attempting to fabricate large arrays of 3D nanostructures in a simple, controllable, and cost-effective manner. Galvanic displacement reactions (GDRs) are electrochemical deposition methods that are well suited for forming high-purity, complex metallic and semiconducting nanostructures with controlled crystallinity, crystal structures, good substrate adhesion, and excellent substrate selectivity.[5,6] In a GDR, the metal ions in the electrolyte are reduced by the substrate itself upon immersion, and no external current source or reducing agent needs to be added to the bath.

Trigonal tellurium (t-Te) has been used as a proof of concept material to form 3D nanostructures because it can readily form one-dimensional (1D) structures both with and without templates and surfactants.[7] It has a highly anisotropic crystal structure consisting of helical chains of covalently bound atoms, which are bound together through van der Waals interactions in a hexagonal lattice. This results in the consistent growth of the crystals along the c-axis, and these crystals have a marked tendency to form 1D nanostructures.[8,9] In addition, t-Te, which has a narrow direct band gap (~0.35 eV), exhibits many interesting properties such as photoconductivity, thermoelectricity, piezoelectricity, catalytic activity, and nonlinear optical properties.[10,11,12,13] These unique properties of 1D Te nanostructures allow them to be used in many applications, including in gas sensors, electronic and optoelectronic devices.[14,15,16]

In this study, we synthesized 3D Te–Si heterostructures with controlled shapes and morphologies by combining two electrochemical methods, namely, the selective metal-assisted chemical etching (MACE) of Si to form Si nanotrunks and a GDR of Si to form Te branches or nanoleaves, under ambient conditions. Unlike other synthesis methods, these processes are highly scalable and compatible with conventional Si processes. In addition, preliminary experiments on photoelectrochemical cells (PECs) based on the fabricated nanostructures indicated that the hyperbranched heterostructures are highly efficient active materials because of their ability to decouple the directions of light absorption and charge-carrier collection.[17,18]

2 Experimental

2.1 Sample preparation

Figure 1 illustrates the fabrication steps used to form the Te–Si heterostructures. The single-crystalline, boron-doped, and (100)-

oriented Si (electrical resistivity of 1–10 Ω cm) wafers (Shijazhuang Xudao Co., China) used as substrates were cleaned using the standard RCA cleaning procedure prior to the formation of ordered layers of polystyrene (PS) beads, which were used as templates.[19] Monodispersed PS beads with a mean diameter of 500 nm were employed to form a hexagonal, close-packed, monolayered array on the Si substrate (Supplementary Information, Fig. S1a). The PS bead solution (10% w/w in water, Thermo Scientific, USA) was mixed with ethanol in a volume ratio of 1:1. The solution was then carefully injected onto the water–air interface with a syringe and treated with 0.5 µl of Triton-X 100 (Sigma-Aldrich, USA) to form the hexagonal, close-packed PS monolayer. Details of the monolayer formation process can be found in the literature.[20] The PS monolayer was treated with an oxygen plasma (Standard Asher RIE System, SNTEK, Korea) to reduce the diameter of the PS spheres to the desirable level. The O_2 gas flow rate and the input power were kept at 200 sccm and 300 W, respectively, whereas the treatment time was fixed at 10 s. This reduced the diameter of the PS beads to 450 nm. Subsequently, 20-nm-thick Au thin films were thermally deposited (VTR-5000, SNTEK, Korea) onto the size-reduced PS-masked Si substrates (Supplemental Information, Fig. S1b). The PS bead masks were lifted off through sonication in ethanol for 10 s, and the Au-patterned Si substrates were immersed in a chemical etching solution (20 ml of 30% H_2O_2, 120 ml of 50% HF, and 1200 ml of 99% ethanol) for 1 to 2 h to adjust the length of the Si trunks from approximately 1 to 2.3 µm. After the MACE of the Si substrates, the gold film on each substrate was selectively removed using a gold etchant (GE8148, Transene Company Inc., USA). Prior to the GDR, the arrays of Si nanotrunks were degreased with isopropyl alcohol (IPA), and the native SiO_2 layers were etched using 10% HF for 5 min. The samples were then immersed in an acidic fluoride bath containing $HTeO_2^+$ at room temperature in the absence of stirring. Two different electrolytes (1 mM $HTeO_2^+$ + 4.5 M HF and 1 mM $HTeO_2^+$ + 1 M $CdCl_2$ + 4.5 M HF) were used to form Te nanostructures of different shapes (*i.e.,* Te nanoleaves and nanobranches). After the GDR, the synthesized Te–Si hybrid nanostructures were carefully rinsed several times with deionized water and IPA.

2.2 Characterization and measurement

The crystal structure and crystallinity of the galvanically displaced Te nanostructures fabricated on the Si nanotrunks were characterized by X-ray diffraction (XRD) analyses (DMAX2500, Rigaku, Japan) which were performed using Cu K_α radiation (λ = 1.5406 Å). The morphologies and microstructures were examined using field-emission scanning electron microscopy (FESEM) (S-4800, Hitachi, Japan) and transmission electron microscopy (TEM) (JEM-2100F, JEOL, Japan), respectively. Raman scattering spectroscopy data were obtained at room temperature using a Jobin Yvon Horiba (Japan) LabRAM system in the confocal configuration. The 514.5 nm line of an argon ion laser was employed for the characterization of the galvanically displaced Te nanostructures. The photoelectrochemical measurements were performed using a three-electrode configuration with 0.02 M K_2SO_4 as the electrolyte solution. The measurements were made under incident light from a 500 W xenon lamp (Oriel, Newport, USA); the light was made to pass through an AMG 1.5 filter. The structure of the photoelectrochemical cell fabricated using the synthesized nanostructures was a solid-state, multilayered one. It consisted of the Te nanoleaves or nanotrees fabricated on a p-type Si substrate, whose back side was connected to a Cu ribbon using Ag paste. The Cu ribbon acted as the working electrode. An Ag/AgCl electrode and a piece of Pt foil were used as the reference and counter electrodes, respectively. During the photoelectrochemical measurements, the applied potential was fixed at -0.4 V (vs. saturated Ag/AgCl) using a SP-200 potentiostat (Biologic, USA).

3 Results and discussion

3.1 Synthesis of Si nanotrunk arrays

Figure S1a shows ordered arrays of PS beads with a mean diameter of ~500 nm on a (100) Si substrate. The arrays of the periodically arranged particles were formed by the self-assembly of the polymer nanospheres into a closely packed monolayer, which acted as a material deposition mask. A few smaller beads disturbed particles in different locations, causing deviations from a perfect hexagonal, close-packed pattern. After the oxygen plasma treatment, the diameter of the PS beads could be effectively reduced. The average diameter of the reduced PS spheres was approximately 450 nm, as shown in Fig. S1b. The periodic arrays of the non-close-packed PS spheres were then used as a shadow mask for the deposition of the Au catalytic layer. Owing to the non-close-packed PS monolayer mask, the Au thin film, which passed through the interstices in the PS mask, was deposited on the substrate in the shape of a hexagonal array. The subsequent removal of the PS nanosphere mask by sonication resulted in a connected and triangular Au film with an array-like structure. Using this Au array-like film as the etching catalyst, ordered Si nanotrunk arrays could be produced by etching the Si wafer in a solution containing H_2O_2, HF, and ethanol.[21,22] The etching process occurred as a localized electrochemical one, with the nanometer-sized metal structures acting as local cathodes. Microscopically, a galvanic cell was formed where Au and Si acted as the local cathode and anode, respectively.

After the completion of the Au-assisted selective electrochemical etching process, the Si substrates turned dark black because light scattered from them owing to their surface roughness.[21] Figures S2a–c show typical SEM images of the synthesized Si nanotrunk arrays. As can be seen from Fig. S2, well-ordered, vertically aligned arrays of Si nanotrunks with a uniform diameter were fabricated successfully. The average bottom diameter of the Si nanotrunks was approximately 400 nm, which was similar to the size of the PS bead masks. High-resolution SEM images showed that the size distribution of the Si nanotrunks protruding from the Au nanoholes corresponded closely to the size distribution of the Au nanoholes. Because the dimensions of the Au nanoholes were controlled by the PS masks, it was possible to tune the diameters and packing densities of the Si nanotrunks by varying the size of PS particles. In addition, it was anticipated that PS beads with a greater uniformity would yield Si nanotrunks with a narrower size distribution. The Si nanotrunks were conical; this might be a

result of the isotropic electrochemical etching of the Si substrates. The length of the Si trunks was controlled by adjusting the etching time (Fig. S2d). As expected, the length of the trunks increased monotonically with an increase in the etching time. This was attributable to the lowering of the diffusion rate of the reactive species as the pore length increased.

3.2 Controlling the morphology of Te nanostructures on Si nanotrunks

Te nanostructures were synthesized on the Si nanotrunks by immersing the substrate in a GDR solution at room temperature in the absence of agitation. As was the case for the electrochemical etching of Si by Au, the driving force for the GDR is the difference in the redox potentials of the sacrificial material (*i.e.,* Si) and the noble metal ions (*i.e.,* $HTeO_2^+$):[23,24]

$$Si(s) + 6F^-(aq) \rightarrow SiF_6^{2-}(aq) + 4e^-$$
$$E^0(Si^{4+}/Si^0) = -1.20 \text{ V vs. NHE} \quad (1)$$
$$HTeO_2^+(aq) + 3H^+(aq) + 4e^- \rightarrow Te(s) + 2H_2O$$
$$E^0(HTeO_2^+/Te) = 0.551\text{V vs. NHE} \quad (2)$$

$$Si(s) + 6F^-(aq) + HTeO_2^+(aq) + 3H^+ \rightarrow SiF_6^{2-}(aq) + Te(s) + 2H_2O \quad (3)$$

During the reaction, both anodic and cathodic reactions occurred simultaneously on the Si surface, with the charge being exchanged through the substrate.[25,26] Fluoride ions furthered the dissolution of Si by forming soluble silicon hexafluoride instead of silicon dioxide.[27]

As shown in Fig. 2, Cd^{+2} ions had a strong effect on the morphology of the Te nanostructures during the GDR. In the absence of Cd^{+2} ions, Te was deposited in a nodular shape (Figs. 2a and b), whereas branch-like Te nanostructures were formed in the presence of Cd^{+2} ions (Figs. 2c and d). To determine the preferred growth orientation of the Te–Si hybrid nanostructures, their X-ray diffraction patterns were examined (Fig. 3). All the diffraction peaks could be indexed to the hexagonal phases of Te (JCPDS Card No. 036-1452). Among these peaks, the (101) peak showed a high intensity, indicating that the Te branches grew along this direction. The Cd^{+2} ions might have acted as a capping reagent; they were bound to the (101) facets more strongly than to the other facets. Thus, Te atoms could be added to the (101) facets readily, resulting in the preferential growth of the Te nanostructures normal to the (101) plane of the crystal lattice.[28] Figures 4 and 5 show TEM and high-resolution TEM (HRTEM) images of the Te–Si hybrid nanostructures formed with and without Cd^{+2} ions in the solution, respectively. The Te nanoleaves were defect-free single crystals that grew preferentially along the (101) and (100) atomic planes and exhibited lattice spacings of approximately 0.328 nm and 0.388, respectively, as shown in Fig. 4. The HRTEM image in Fig. 5 shows that the Te nanobranches grown with the aid of Cd^{+2} ions had a periodic fringe spacing of 0.335 nm along the longitudinal axis of the nanorods; this corresponded to the interplanar spacing between the (101) plane of the hexagonal Te. This indicated that the Te nanorods grew preferentially normal to the (101) plane, resulting in the formation of the nanobranches. The electron diffraction pattern (Fig. 5c) could be indexed to the hexagonal structure; this result was consistent with the results of the XRD analysis.

3.3 Optical properties of Te–Si hybrid nanostructure arrays

Figures 6a and b show the photoluminescence (PL) and Raman spectra, respectively, of the Te nanostructures synthesized using Cd^{+2}-containing and Cd^{+2}-free electrolyte solutions at room temperature. The peak at approximately 400 nm was observed possibly owing to the nanoscaled structure of the Te leaves.[29] The peak at approximately 560 nm could be assigned to a forbidden direct transition as a result of the presence of defect states.[30,31] Nanobranched Te exhibited a low-intensity PL spectrum, which might be the result of efficient charge separation.[32] Three distinctive vibration peaks were observed, at 89.9, 118.7, and 137.9 cm^{-1}, in the Raman spectra, which corresponded to the *E* bond-stretching, A_1 bond-stretching, and *E* bond-stretching modes, respectively. These symmetric, sharp, and broad Raman spectra peaks of the Te nanostructures were consistent with the results of the XRD and HRTEM analyses and suggested that the Te nanostructures were highly crystalline and free of impurities. In the case of the Te nanoleaves, however, the characteristic vibration peaks were red-shifted to 3 nm. On the basis of the Campbell and Fauchet model, the fact that the peaks corresponding to the Te nanoleaves appeared at a lower frequency and were asymmetric and broader could be attributed to the smaller grain size of the nanoleaves; this was also confirmed by the results of the XRD analysis.

3.4 Photoelectrochemical properties of Te–Si hybrid nanostructure arrays

The photocurrent response of the Te–Si nanotrees under chopped illumination was compared to that of the Te–Si nanoleaves (Fig. 7). In the case of white-light irradiation, the photocurrents of both samples decreased, indicating their *p*-type semiconductor nature.[34] A more prompt photocurrent response with a greater current spike at each cycle was observed from the branched Te–Si heterostructures; this could be ascribed to the fact that the nanotrees contained a greater amount of preadsorbed water and electrolyte, owing to their larger surface area.[35] The photocurrent response of the nanobranched Te–Si heterostructures was approximately two times greater than that of the Te–Si heterostructures with nanoleaves. This could be attributed to more efficient light scattering and the larger surface area of the former. It is possible that the nanobranched structures acted as a light-scattering layer, resulting in a higher photocurrent. Their large surface area also helped increase the photocurrent.[1] Further, Fig. 7 shows that the photoresponse of the nanotrees was reproducible during the light-on and light-off states. No notable changes in the peak shape occurred during the irradiation. This was probably because the decomposition reaction potential was not within the band-gap of the Te material.

4 Conclusions

In summary, we developed a novel approach for synthesizing hybrid Te–Si nanostructures by combining gold-assisted chemical etching and a galvanic displacement reaction of Si. The dimensions of the fabricated Si nanotrunks could be controlled by varying the characteristics of the PS mask and the etching time.

By simply adjusting the electrolyte composition, the Te nanostructures formed on the Si substrate could be controlled to be shaped like nanoleaves or nanobranches. The fabricated Si nanotrunks with Te nanobranches showed stronger luminescent emission in the visible region, as well a higher wave number in the Raman spectra, owing to their larger grain size. The obtained results demonstrated clearly that the optical and photoelectrochemical properties of Te–Si hybrid nanostructures depend on their shape and size. This simple electrochemical approach should be suitable for preparing hierarchical nanostructures for use in photoelectronic and photoelectrochemical devices. Further studies on the electrical, piezoelectric, and photoconductive properties of the thus-fabricated hybrid structures are underway.

Acknowledgements

This work was supported by a grant from the Fundamental R&D Program for Core Technology of Materials and the Energy Efficiency & Resources program of the Korea Institute of Energy Technology Evaluation, Planning (KETEP) (Grant No. 20112010100100), which is funded by the Ministry of Knowledge Economy, Republic of Korea. Support was also provided by the Global Frontier Program through the Global Frontier Hybrid Interface Materials (GFHIM) program (2013M3A6B1078870) of the National Research Foundation (NRF), Korea, which is funded by the Ministry of Science, ICT & Future Planning. Partial support was also provided by the Korean Institute of Materials Science.

Notes and references

[a] *Electrochemistry Department, Korea Institute of Materials Science, Changwon 641-831, Korea.*
[b] *Department of Bionano Technology, Hanyang University, Ansan 426-791, Korea. Fax: +82 31-418-6490; Tel: +82 31-400-5650; E-mail: choa15@hanyang.ac.kr*
[c] *Department of Fusion Chemical Engineering, Hanyang University, Ansan 426-791, Korea. Fax: +82 31-418-6490; Tel: +82 31-400-5650; E-mail: choa15@hanyang.ac.kr*
[d] *Department of Materials Science and Engineering, Seoul National University of Science and Technology, Seoul 139-743, Korea.*
[e] *Advanced Characterization & Analysis Group, Korea Institute of Materials Science, Changwon 641-831, Korea.*
[e] *Advanced Materials and Application Research Division, Korea Electrotechnology Research Institute, Changwon 642-120, Korea.*
[f] *Deparment of Chemical and Environmental Engineering, University of California-Riverside, Riverside, CA 92521, United States. Fax: +1 951-827-5696; Tel: +1 951-827-7710; E-mail: myung@engr.ucr.edu*

† Electronic Supplementary Information (ESI) available: Additional SEM images of the self-assembled PS monolayer and vertically aligned Si nanotrunks. See DOI: 10.1039/b000000x/

[+] These authors contributed equally to this work.

1 N. Dasgupta and P. Yang, *Front. Phys.*, 2013, **2**, 1.
2 C. Lai, Q. Wu, J. Chen, L. Wen and S. Ren, *Nanotechnology*, 2010, **21**, 215602.
3 S. O. Cho, E. J. Lee, H. M. Lee, J. G. Kim and Y. J. Kim, *Adv. Mater.*, 2006, **18**, 60.
4 P. J. Pauzauskie and P. Yang, *Mater. Today*, 2006, **9**, 36.
5 G. D. Moon, S. Ko, Y. Min, J. Zeng and Y. Xia, U. Jeong, *Nano Today*, 2011, **6**, 186.
6 C. H. Chang, Y. Rheem, Y.-H. Choa, D.-Y. Park and N. V. Myung, *Electrochim. Acta*, 2010, **55**, 1072.
7 S. Wang, W. Guan, D. Ma, X. Chen, L. Wan, S. Huang and J. Wang, *CrystEngComm*, 2010, **12**, 166.
8 A. v. Hippel, *J. Chem. Phys.*, 1948, **16**, 372.
9 E. J. Weidmann and J. C. Anderson, *Thin Solid Films*, 1971, **7,** 265.
10 D. Redfield, *Phys. Rev.*, 1955, **100**, 1094.
11 W. B. Gandrud and R. L. Abrams, *Appl. Phys. Lett.*, 1970, **17**, 302.
12 A. S. Epstein, H. Fritzsche and K. Lark-Horovitz, *Phys. Rev.*, 1957, **107**, 412.
13 J. P. Hermann, G. Quentin and J. M. Thuillier, *Solid State Commun.*, 1969, **7**, 161.
14 Z. Wang, L. Wang, J. Huang, H. Wang, L. Pan and X. Wei, *J. Mater. Chem.*, 2010, **20**, 2457.
15 H. Hirai, H. Sekiguchi, S. Miyata and S. Kobayashi, *Appl. Phys. Lett.*, 1987, **50**, 818.
16 W. Xu, J. Song, L. Sun, J. Yang, W. Hu, Z. Ji and S-H. Yu, *Small*, 2008, **4**, 888.
17 K. Shankar, J. I. Basham, N. K. Allam, O. K. Varghese, G. K. Mor, X. Feng, M. Paulose, J. A. Seabold, K.-S. Choi and C. A. Grimes, *J. Phys. Chem. C*, 2009, **113**, 6327.
18 S. Brittman, H. Gao, E. C. Garnett and P. Yang, *Nano Lett.*, 2011, **11**, 5189.
19 W. Kern, *J. of Electrochem. Soc.*, 1990, **137**, 1887.
20 W. Kandulski, Ph.D. Thesis, University of Bonn, 2007.
21 X. Li and P. W. Bohn, *Appl. Phys. Lett.*, 2000, **77**, 2572.
22 K. Peng, M. Zhang, A. Lu, N.-B. Wong, R. Zhang and S.-T. Lee, *Appl. Phys. Lett.*, 2007, **90**, 163123.
23 F. Xiao, B. Yoo, K. H. Lee and N. V. Myung, *J. Am. Chem. Soc.*, 2007, **129**, 100689.
24 H. Suh, H. Jung, C. M. Hangarter, H. Park, Y. Lee, Y. Choa, N. V. Myung and K. Hong, *Electrochim. Acta*, 2012, **75**, 201–207.
25 Z. Galus, in *Standard Potentials in Aqueous Solution*, ed. A. J. Bard, R. Parsons and J. Jordan, Marcel Dekker, New York, 1985, pp. 220–235.
26 F. Xiao, B. Yoo, M. A. Ryan, K.-H. Lee and N. V. Myung, *Electrochim. Acta*, 2006, **52**, 1101.
27 Z. P. Huang, N. Geyer, P. Werner, J. de Boor and U. Gosele, *Adv. Mater.*, 2011, **23**, 285–308.
28 J. Joo, B. Y. Chow, M. Prakash, E. S. Boyden and J. M. Jacobson, *Nat. Mater.*, 2011, **10**, 596.
29 H.-S. Qian, S.-H. Yu, J.-Y. Gong, L.-B. Luo and L.-F. Fei, *Langmuir*, 2006, **22**, 3830.
30 U. K. Gautam and C. N. R. Rao, *J. .Mater. Chem.*, 2004, **14**, 2530.
31 A. N. Tiwari, D. K. Pandya and K. L. Chopra, *Thin Solid Films*, 1985, **130**, 217.
32 U. Woggon, H. Giessen, F Gindele, O. Wind, B. Fluegel and N. Peyghambarian, *Phys. Rev. B*, 1996, **54,** 17628.
33 V. Swamy, B. C. Muddle and Q. Dai, *Appl. Phys. Lett.*, 2006, **89**, 163118.
34 R. P. Wijesundera, M. Hidaka, K. Koga, M. Sakai, W. Siripala, J.-Y. Choi and N. E. Sung, *Phys. Status Solidi B*, 2007, **244**, 4629.
35 Y. Han, S. Zhang, H. Zhao, W. Wen, H. Zhang, H. Wang and F. Peng, *Langmuir*, 2009, **26**, 6033.
36 M. A. Butler and D. S. Ginley, *J. Mater. Sci.*, 1980, **15**, 1.
37 M. Pourbaix, in Atlas of Electrochemical Equilibria in Aqueous Solutions, Pergamon Press, Oxford, 1st edn., 1974, pp. 560–571.

Figure captions

Fig. 1 Schematic illustration of Te–Si hybrid nanostructures synthesized by selective metal-assisted chemical etching (MACE) of Si to form Si "trunks," followed by galvanic displacement reaction (GDR) of Si to form Te.

Fig. 2 SEM images of Te–Si heterostructures formed by GDR: (a,b) without and (c,d) with Cd ions in the solution.

Fig. 3 XRD patterns of Te–Si heterostructures formed by GDR with and without Cd ions in the GDR solution

Fig. 4 (a) TEM image and (b) high-resolution TEM image of a single nanoleave after GDR in the absence of Cd ions, and (c) and (d) are a lattice image extracted from the part marked by a square in (b) and an FFT pattern, respectively.

Fig. 5 (a) TEM image and (b) high-resolution TEM image of a single nanotree after GDR in the presence of Cd ions, and (c) and (d) are a lattice image extracted from the part marked by a square in (b) and an FFT pattern, respectively.

Fig. 6 (a) Photoluminescence emission spectra with an excitation wavelength of 325 nm, and (b) Raman scattering spectra of Te–Si hybrid nanostructures

Fig. 7 Comparison of photoelectrochemical properties of Te–Si hybrid nanostructures.

Figure 1

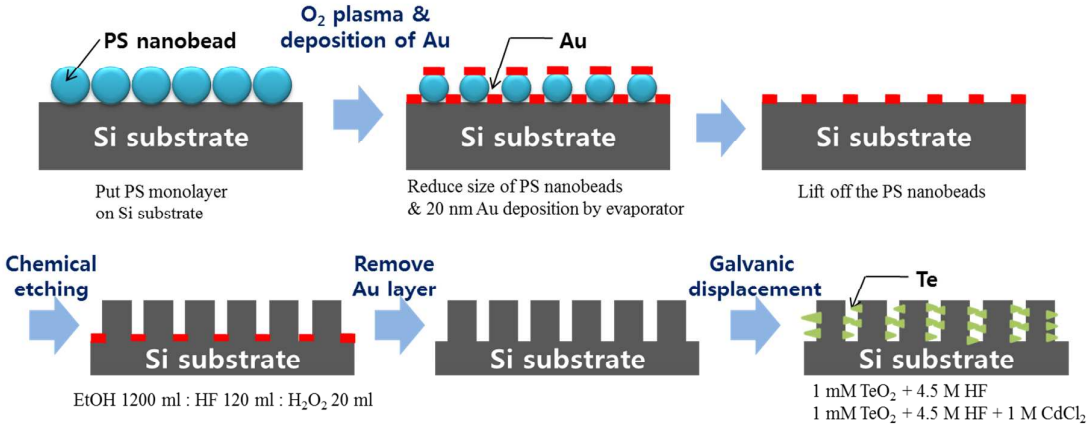

Figure 2

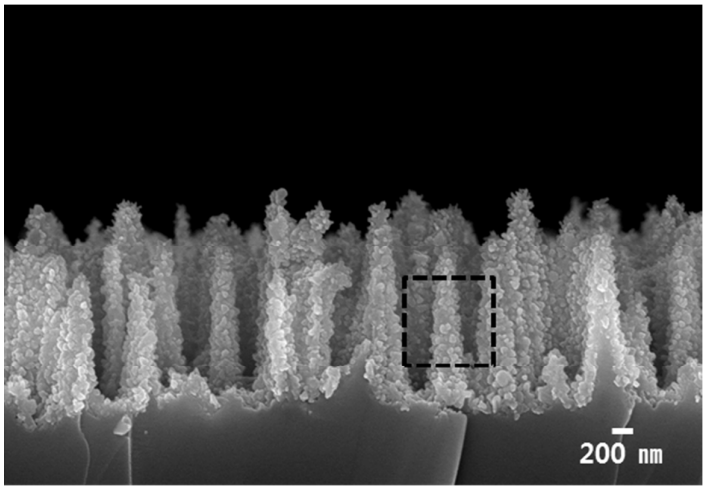

(a)

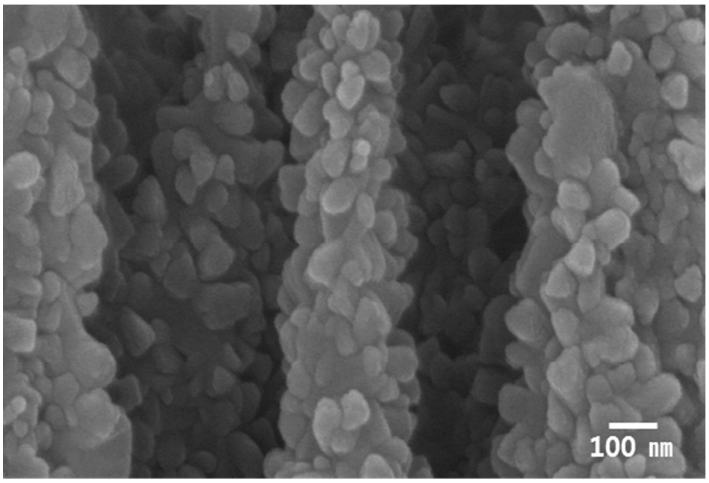

(b)

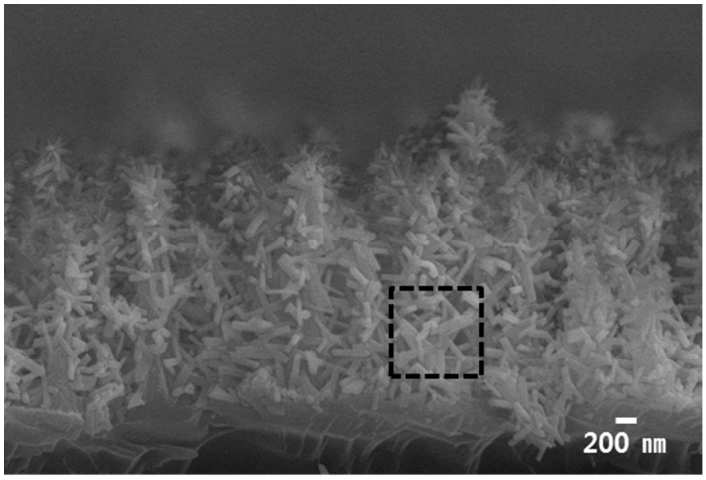

(c)

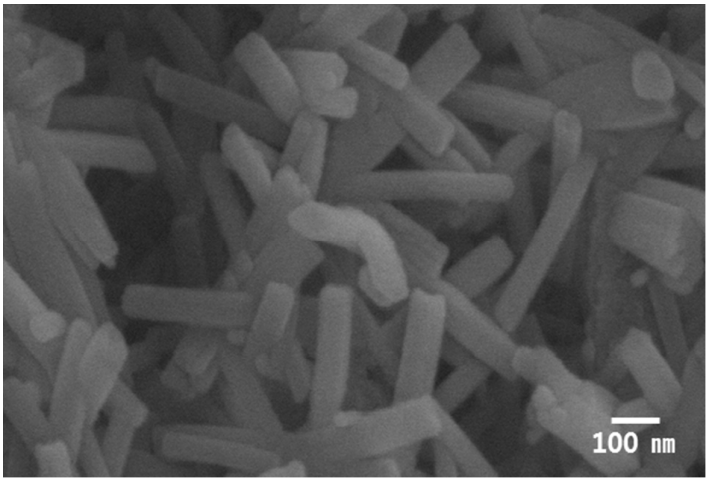

(d)

Figure 3

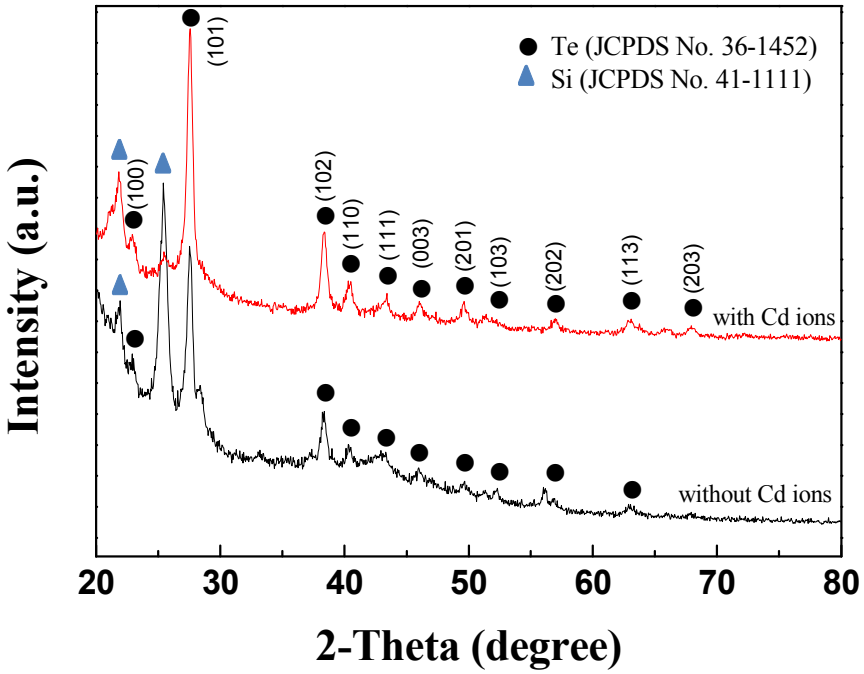

Figure 4

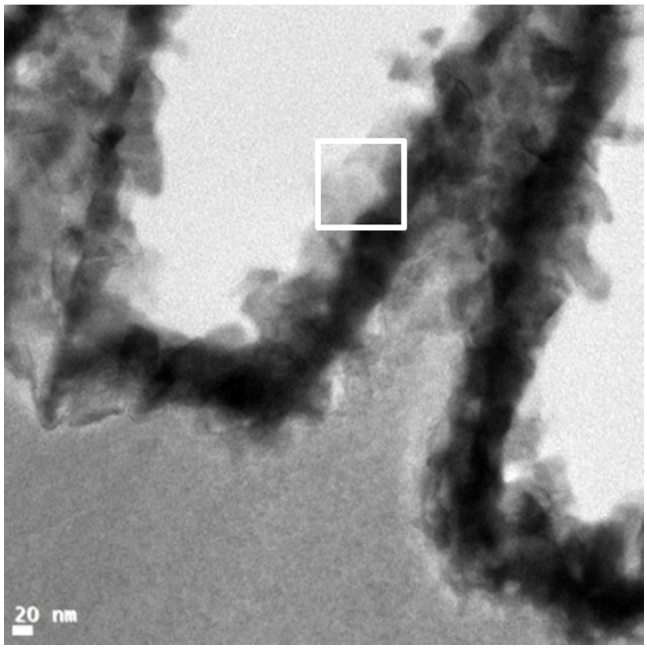

(a)

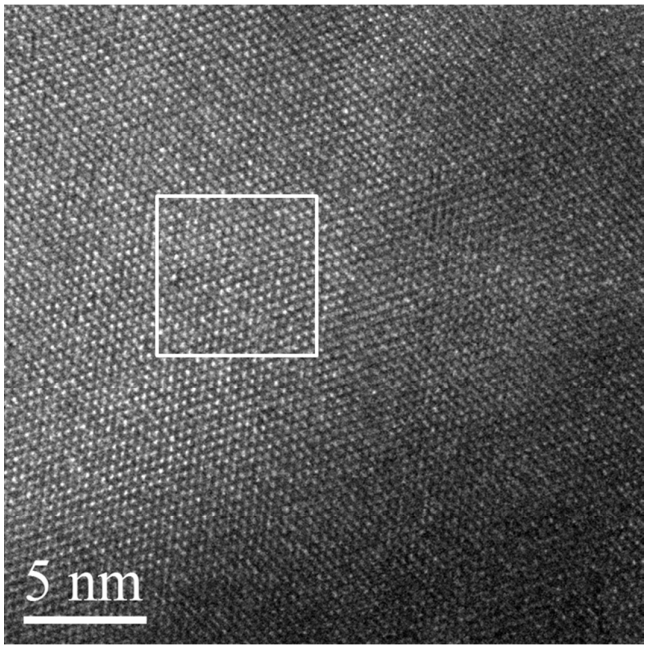

(b)

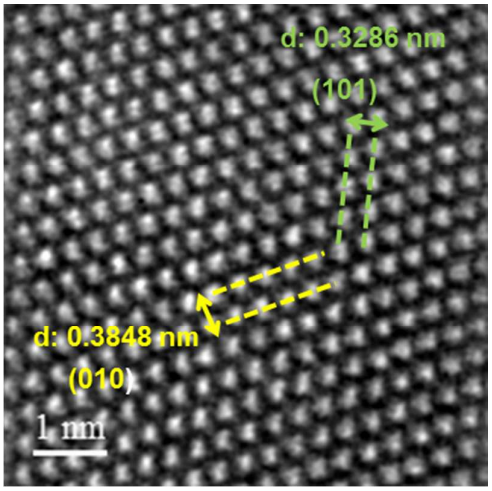

(c)

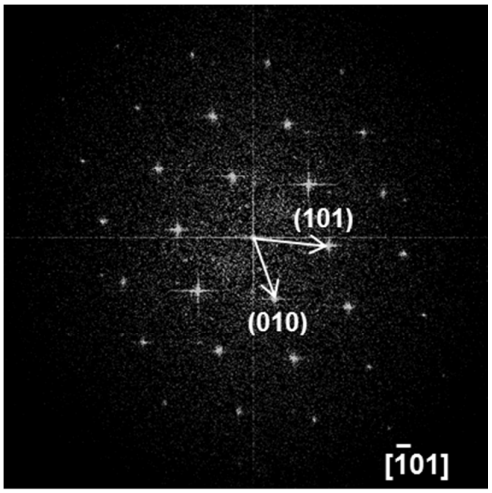

(d)

Figure 5

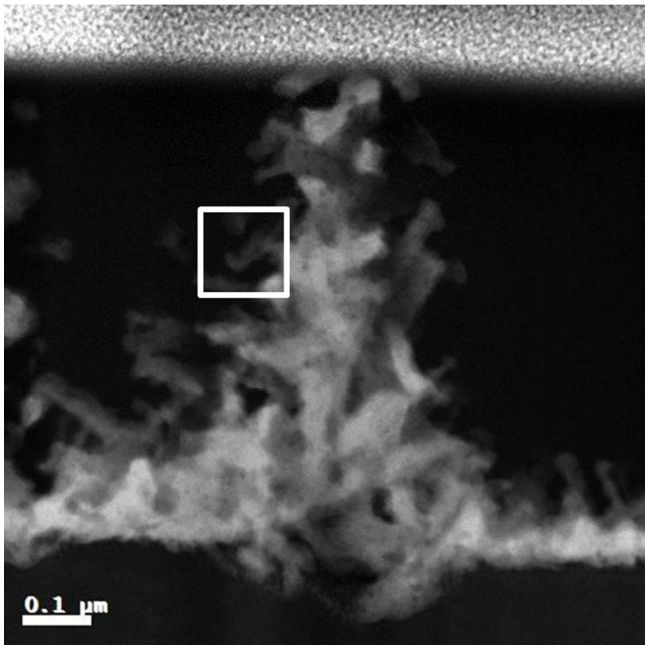

(a)

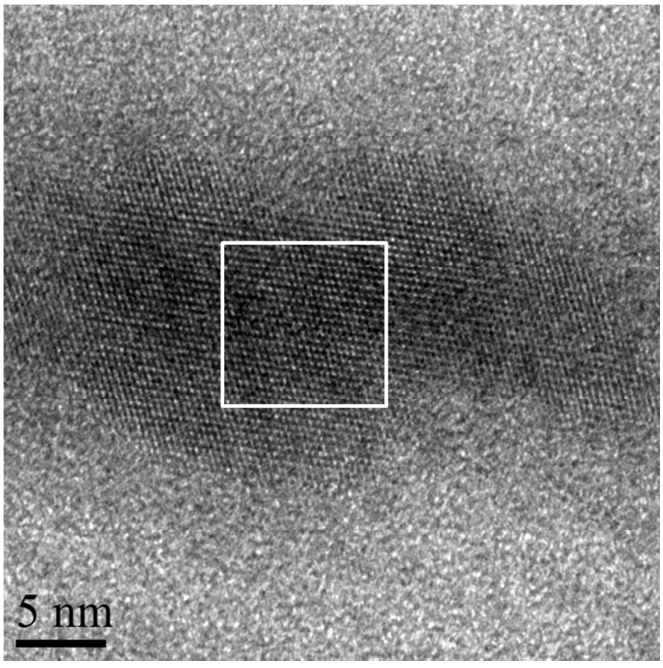

(b)

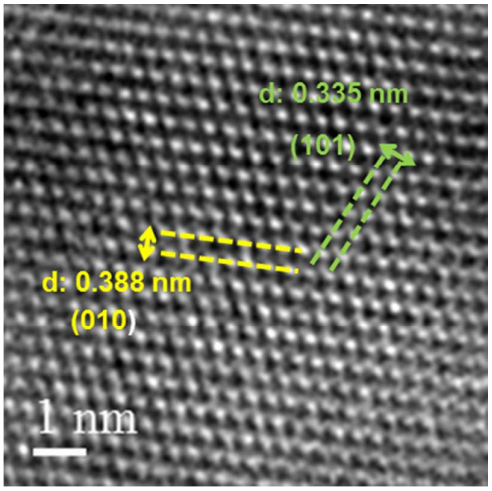

(c)

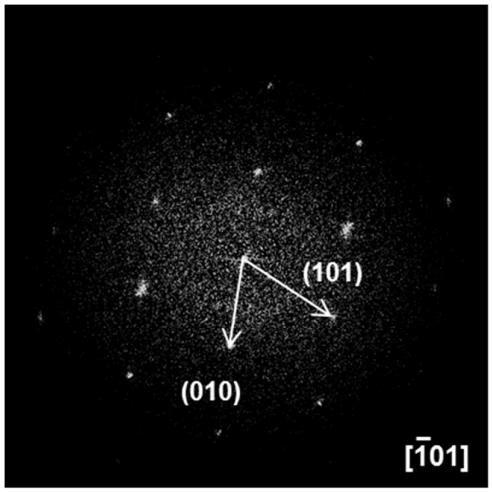

(d)

Figure 6

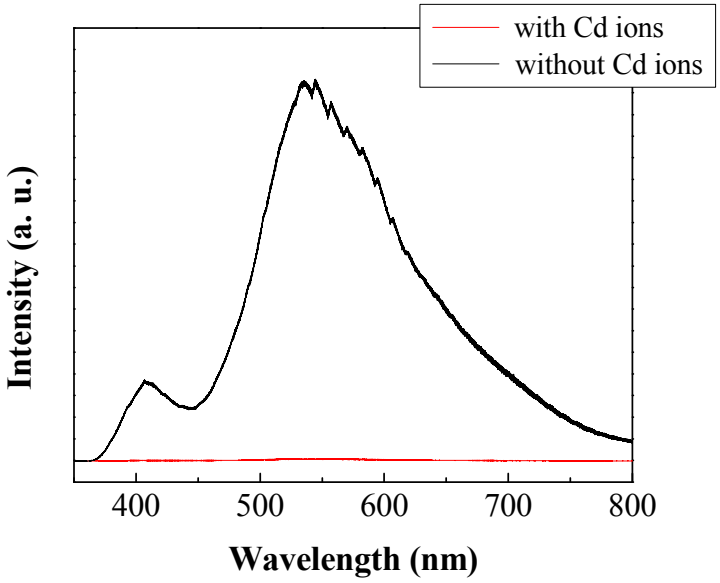

(a)

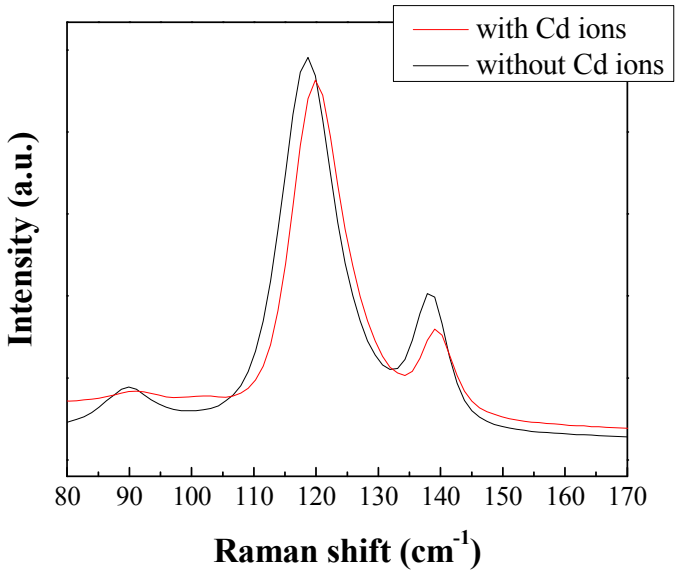

(b)

Figure 7